Silicon resonant microcantilevers for absolute pressure measurement

Silicon resonant microcantilevers for absolute pressure measurement

S. Bianco, M. Cocuzza,[a] S. Ferrero, E. Giuri, G. Piacenza, C. F. Pirri, A. Ricci, and L. Scaltrito
χ Laboratory, Materials and Microsystems Laboratory, Polytechnic of Turin, Lungo Piazza D'Armi 6, Chivasso, Turin 10034, Italy

D. Bich, A. Merialdo, and P. Schina
Olivetti I-Jet, Loc. Le Vieux, Arnad, 11020 Aosta, Italy

R. Correale
Varian SpA, Via Fratelli Varian 54, Leinì, 10040 Turin, Italy

(Received 15 December 2005; accepted 19 May 2006)

This work is focused on the developing of silicon resonant microcantilevers for the measurement of the absolute pressure. The microcantilevers have been fabricated with a two-mask bulk micromachining process. The variation in resonance response of microcantilevers was investigated as a function of pressure (10^{-1}–10^{5} Pa), both in terms of resonance frequency and quality factor. A theoretical description of the resonating microstructure is given according to different molecular and viscous regimes. Also a brief discussion on the different quality factors contributions is presented. Theoretical and experimental data show a very satisfying agreement. The microstructure behavior demonstrates a certain sensitivity over a six decade range and the potential evolution of an absolute pressure sensor working in the same range. © *2006 American Vacuum Society.*
[DOI: 10.1116/1.2214698]

I. INTRODUCTION

The recent scientific and technological advances in microtechnologies have produced an increasing interest in the application of micromechanical freestanding structures (cantilever, bridges, and diaphragms) in many fields where advanced performances, increased sensibility, and reduced dimensions are required: thermal, acceleration, and pressure sensors,[1–3] environmental monitoring,[4–7] biochemical analysis, and[8–12] advanced instruments for surface characterizations.[11,12]

The cantilever structure, in particular, a single-clamped beam, revealed to be the most studied thanks to its wide range of fields of applicability and technological manufacturing processes, which range from surface micromachining,[3,13] which implies the removal of a sacrificial layer and the solution of the stiction problem,[14] to front[4,15,16] or backside[5] bulk micromachining. In any case most of the technological processes depicted in literature require the deposition of a structural film on a silicon substrate,[3,4,13,15] with consequent thermal expansion coefficient mismatch which results in stress or bending of the final structure. Some solutions have been proposed (low stress silicon nitride deposition, postrelease annealing process, etc.),[14,17] but we choose to fabricate a cantilever structure based on the same silicon substrate and with a backside bulk micromachining technique. The process is not novel but it avoids stress or stiction problems.

For what concerns the mode of operation, two approaches appear to be consolidated in literature: a static or dc operation mode[8,10] (the cantilever bends when subjected to stress due to external mass adsorption or thermal phenomena), basically involved in biological screening, and a dynamic or ac operation mode[1,8,9] (the cantilever resonance frequency and quality factor shift due to mass loading or variations of environmental damping conditions), applied both for biomedical and pressure measurements.

Aim of this work is the fabrication of resonant microcantilevers for the measurement of absolute pressure[1,2] over a range of six decades, from atmospheric pressure down to 10^{-1} Pa [which can be considered fairly wide if compared with previous microelectromechanical sytstem (MEMS) based solutions] by monitoring the shift of both the resonance frequency and the quality factor according to the variations of ambient damping connected with the variations of pressure.

II. CANTILEVER PROCESS AND SIMULATION

Arrays of rectangular silicon cantilever structures have been fabricated through MEMS techniques by using a reactive ion etching (RIE) technique on the front of the wafer, for the definition of the cantilever shape, and a backside bulk micromachining technique for the release of the cantilever structure (two-mask process).

The process is illustrated in Fig. 1. (100)-oriented silicon wafers with a thermally grown 500 nm thick SiO_2 layer on both sides were used as starting substrates [Fig. 1(a)]. RIE of SiO_2 and silicon was used on the front of the wafer to define the cantilever array geometry [first mask, Figs. 1(b) and 1(c)]. A thermal oxidation was performed to produce a 500 nm thick SiO_2 etch-stop layer on the lateral sides and at the bottom of the square window hosting the cantilever array [Fig. 1(d)]. Then, access to the backside silicon was obtained through buffered hydrofluoridric (BHF) acid wet etching of the back SiO_2 masking layer [second mask, Fig. 1(e)], which

[a]Electronic mail: matteo.cocuzza@infm.polito.it

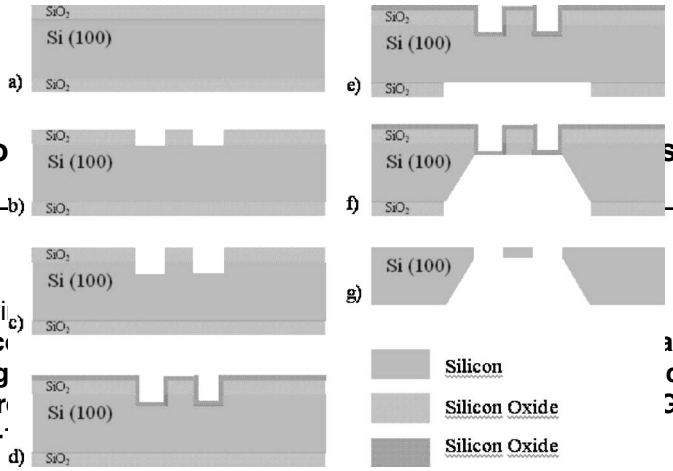

FIG. 1. Process steps for the fabrication of the cantilevers (schematic cross section): (a) wafer thermal oxidation; (b) RIE of front silicon oxide layer; (c) RIE of front side silicon; (d) thermal oxidation of the bottom of the exposed silicon square window and lateral sides of the cantilever; (e) BHF wet etching of the back silicon oxide layer; (f) TMAH anisotropic etching on the back of the silicon substrate; (g) cantilever release by BHF dipping.

is very selective respect to silicon. A time controlled tetra-Methylammonium hydroxide (TMAH) anisotropic wet etching, assisted by the front SiO_2 etch-stop layer, was used to produce a thin diaphragm made by SiO_2 and the same silicon array of cantilever [Fig. 1(f)]. The array was finally released by BHF dipping [Fig. 1(g)].

This solution allows the fabrication of cantilevers deriving from the same bulk silicon, with a good control on their thickness (defined by RIE), and most of all, avoiding stress due to structural film deposition. Cantilevers of different dimensions in a fairly wide range were produced (width $w=5-100$ μm; length $l=30-800$ μm; thickness $t=5-20$ μm) to investigate different vibrational properties such as stiffness and oscillation eigenmodes as well as static mode bending for free cantilevers. After a preliminary set of measurements we decided to test only the 5 μm thick cantilevers, because they presented the better response in terms of sensitivity and range of measurement, while the thicker beams were unable to provide good results in a wide range of pressures. Actually a silicon-on-insulator (SOI) wafer solution is under study as an alternative to the described process, to obtain thinner and better controlled cantilevers.

Also simulations of structure behavior have been carried out by means of finite element analysis for design purpose. We used the finite element analysis (FEA) COVENTORWARE™ software to build (process editor), discretize (preprocessor), and simulate (MemMech) the undamped mechanical modal frequencies, mode shapes, and quality factors of the monocrystalline silicon rectangular cantilevers. In simulations we used parabolic brick elements to discretize our system and the mesh optimal density was obtained from convergence studies.

III. BRIEF THEORETICAL DESCRIPTION

We focused our attention on the variation of two measurable parameters, the angular resonance frequency ω_r and the mechanical quality factor Q of the cantilever beam. We can define the quality factor as[18]

$$Q = 2\pi \frac{U_s}{U_d}, \tag{1}$$

where U_s is the stored vibration energy and U_d is the dissipated energy during a period.

There are many ways to evaluate experimentally the quality factor of a vibrating beam (e.g., the logarithmic time decrement of the vibration after a short impulse or the ratio of the vibration amplitude at resonance with respect to the static one). We chose to evaluate the bandwidth at resonance.

Different phenomena contribute to energy dissipation and we can classify loss mechanisms into three categories: (a) external effects, such as the pressure effects on vibration dynamics (and this is the aim of this work); (b) dissipations related to the coupling to the support structure (clamping loss); (c) internal frictions, related to a variety of different physical mechanisms. So the measured Q factor can be divided in every single contribution, such as:[18]

$$\frac{1}{Q_{\text{tot}}} = \sum_i \frac{1}{Q_i}, \tag{2}$$

and obviously the smallest Q_i will dominate.

A. Pressure dependence

It is useful to divide the total pressure range from vacuum to atmospheric pressure into several regions, in which different physical conditions have to be considered. The parameter used to separate these regions is the so-called Knudsen number Kn, defined as[1]

$$\text{Kn} = \frac{\lambda}{w} = \frac{1}{D\sigma w}, \tag{3}$$

where λ is the mean free path of gas molecules, w is the width of the gas layer in motion (that we can approximate with the cantilever width), D is the gas number density, and σ is the collision cross section.

At low pressure we can consider air molecules as noninteracting. In this rarefied gas air molecules interact with the moving surface of the cantilever via elastic collisions and damping is proportional to the cantilever velocity (the dimension of the body is much smaller than the mean free path of moving molecules). The right way to evaluate this effect is using the kinetic theory of gases. This is called free-molecule regime and, in terms of Knudsen number, these conditions are verified for $\text{Kn} > 10$. Very high values of Kn characterize the intrinsic region, in which air damping is negligible and no pressure effects on vibration dynamics are expected.[19]

For higher pressures, the gas properties are dominated by molecule-molecule interactions and air can be considered as a viscous incompressible fluid (in this case the mean free path is much smaller than the dimension of the beam, so we

can consider the gas as a continuum). The damping effect (related to the acceleration of the cantilever) can be calculated using fluid mechanics, solving the Navier-Stokes and continuity equations with slip boundary conditions.[20] This is usually known as viscous region and these conditions are verified for $\mathrm{Kn} < 0.1$

Between the two given values of the Knudsen number there is the transition regime, in which both inertial and noninertial components are present.

B. Molecular region

In molecular-free regime we do not expect any pressure dependence for the resonance frequency value.[1] In this case we can evaluate, using standard mechanics, the undamped angular resonance frequency $\omega_r^{(n)}$, which can be written as[19]

$$\omega_r^{(n)} = k_n^2 \frac{t}{l^2} \sqrt{\frac{E}{12\rho_b}}, \tag{4}$$

where E and ρ_b are Young's modulus and density of the beam material and k_n is the constant for the nth order vibrational mode ($k_0 = 1.875$ for the first resonance mode).

In these conditions the pressure dependence for the quality factor of the cantilever can be evaluated using the Christian model[21] for a rectangular-shape vibrating beam. Two equivalent approaches are proposed, evaluating the momentum transfer rate from the vibrating plate to the surrounding gas due to the collisions between the plate and the molecules, or directly the energy transfer between the gas molecules and the vibrating beam, obtaining the same results.[22] So, for the first resonance mode, we can write the pressure-dependent quality factor Q_p as

$$Q_p = \frac{\rho_b t \omega_0}{4} \sqrt{\frac{\pi}{2}} \sqrt{\frac{RT}{M}} \frac{1}{p}, \tag{5}$$

where $\omega_0 \equiv \omega_r^{(0)}$ is obtained from (5), M, R, and T are the mass of the gas molecules, the gas constant, and the absolute temperature, respectively, and p is the pressure.

This model allows us to estimate the external damping effects in vacuum for a cantilever vibrating in the free space (we do not consider any nearby wall close to the cantilever that produces the so-called squeeze-film damping) and these are the correct boundary conditions for our experimental measurements.

C. Viscous region

In the viscous region we can calculate the damping force using fluid mechanics. If we consider that the speed of the vibrating cantilever is always much smaller than the speed of sound in the medium, we can write the Navier-Stokes equation and the continuity equation for an incompressible fluid.[20]

We cannot solve analytically the problem in the general case, so we have to approximate our physical system to obtain a close-form solution for the damping force. The usual model (proposed by Kokubun *et al.*[23] to study the damped motion of a vibrating quartz tuning fork) suggests to describe the system as a string of oscillating spheres with diameter equal to the width of the oscillator. In this case, considering a small Reynolds number, the drag force components can be calculated.

Now we are able to obtain the pressure-dependent relations for the angular resonance frequency ω_r and the mechanical quality factor Q_p in the viscous regime. Blom *et al.*[19] used a simplified version of the method described above to calculate the two parameters (they considered a single oscillating sphere, with radius R equal to the width w of the cantilever). Hosaka *et al.*[24] refined the model *et al.*: they represented, as Kokubun *et al.* did, the cantilever as a string of spheres, with the diameter (not the radius) equal to the geometrical width of the beam.

Using the results obtained by Hosaka *et al.*, we can calculate the normalized variation of the angular resonance frequency, and our result is

$$\frac{\Delta\omega(p)}{\omega_0} = \frac{\omega_r(p) - \omega_0}{\omega_0} = -\frac{\pi w}{24\rho_b t} \frac{M}{RT} p - \frac{3\pi}{8\rho_b t} \sqrt{2\mu \frac{M}{RT}} \sqrt{\frac{p}{\omega_0}}, \tag{6}$$

where μ is the dynamic viscosity. Furthermore Hosaka *et al.* gave a direct evaluation of the quality factor Q_p,

$$Q_p = \frac{2\rho_b t w^2 \omega_0}{6\pi\mu w + (3/2)\pi w^2 \sqrt{2\mu(M/RT)\omega_0 p}}. \tag{7}$$

We can see from Eq. (7) that, on the first part of the viscous region (low pressure), there is a weak dependence on pressure while, when pressure rises, the $1/\sqrt{p}$ dependence dominates. Blom *et al.* strongly underline this aspect, dividing the viscous zone in two parts, the first one in which Q_p is independent of p and the second one in which Q_p is proportional to $1/\sqrt{p}$.

Equations (6) and (7) are obtained considering only a translational motion, not a torsional one; however, it is reasonable to suppose that energy dissipation related to a torsional mode of vibration can be neglected without introducing an important error in the analysis.[24]

D. Other contributions to the quality factor

Until now we focused our attention only to the pressure-related contribution to the mechanical quality factor, but, according to (2), every dissipation mechanism can play a role in the definition of Q. In literature many loss contributions are analytically described, such as clamping effects, thermoelastic damping effects (TDEs), internal friction, and surface effects.[18,25–27]

The coupling to the support structure causes a dissipation of vibrational energy of the cantilever, and this effect is known as clamping loss. Clamping effects are completely described by Hao *et al.*[25] obtaining a close-form model for support loss both for clamped-free (which is our case of interest) and clamped-clamped micromachined beam resona-

tors with in-plane flexural vibration. We can write the analytical solution Q_c, with an explicit dependence on geometry, as

$$Q_c = \gamma_n \left(\frac{l}{t}\right)^3, \tag{8}$$

where γ_n is a constant (related to the nth order vibration mode) which depends only on the beam material. For a single-crystal silicon cantilever and for the first mode we have $\gamma_0 \cong 2.232$.

Other dissipative effects are caused by internal frictions. One of these loss contributions is the thermoelastic energy dissipation (TED).[26] During the oscillation of the beam the region under compression will warm while the region under expansion will cool, creating a temperature gradient and consequently an irreversible heat flow across the cantilever thickness. Lifshitz *et al.*[26] calculated the TED contribution Q_{TED}, obtaining

$$Q_{\mathrm{TED}}^{-1} = \frac{E\alpha_T^2 T}{C_p \rho_b}\left[\frac{6}{\xi^2} - \frac{6}{\xi^3}\frac{\sinh(\xi)+\sin(\xi)}{\cosh(\xi)+\cos(\xi)}\right],$$
$$\xi = w\sqrt{\frac{\rho_b C_p \omega_0}{2k}}, \tag{9}$$

where α_T is the coefficient of thermal expansion of the cantilever material, T is the absolute temperature of the environment, C_p is the specific heat, and k is the thermal conductivity.

The last contributions to the quality factor that we have to take into account derive from volume (bulk) and surface effects. The bulk loss can be studied introducing a complex-valued Young's modulus $E_c = E + iE_d$, where E is the conventional (real-valued) Young's modulus and E_d represents the dissipative part.[18] Yasumura *et al.*[18] gave a simple relation for Q_{volume} (which is independent of cantilever geometry and vibrational mode shape),

$$Q_{\mathrm{volume}} = \frac{E}{E_d}. \tag{10}$$

To study the surface losses Yang *et al.*[27] supposed that a thin surface layer is formed on the beam (for example, a native silicon oxide layer on a single-crystal silicon cantilever), creating a surface stress that leads to an energy dissipation. If we consider a layer with thickness δ and a complex Young's modulus $E_{cs} = E_s + iE_{ds}$, on the top of a bulk material (with the same notation for the bulk Young's modulus used above), the relation for Q_{surface} can be written as

$$Q_{\mathrm{surface}} = \frac{wt}{2\delta(3w+t)}\frac{E}{E_{ds}}. \tag{11}$$

IV. EXPERIMENTAL SETUP

In our experimental measurements we monitored the variation of the resonance frequency and the quality factor due to pressure-related damping processes, so we worked in the so-called ac mode. For the excitation of the microstructures, a small piezoelectric disk was used. A function generator (HP 33120A) produced a square wave signal that was amplified and sent to the piezoelectric actuator, to give us the possibility to control the frequency of the oscillation. The actuator was linked to a holding cell, the test die with the array of cantilevers was attached to the actuator with double-sided tape, and the cell was evacuated by a series of a membrane and turbomolecular pump (MINI-Task System, Varian Inc. Vacuum Technologies). A needle valve with incorporated micropositioner was used to maintain a precise level of pressure, ranging from 10^{-3} Pa to atmospheric pressure. Two capacitive sensors (MKS Baratron) provided an accurate evaluation of the pressure value in the analysis chamber.

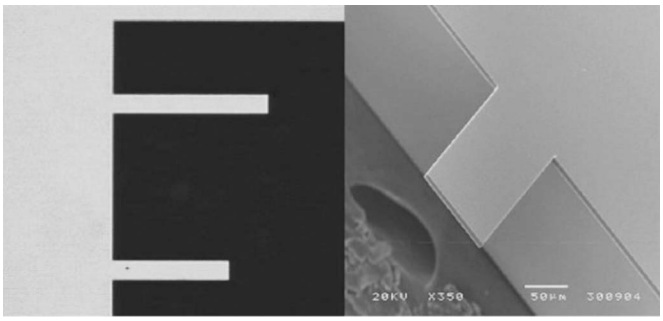

FIG. 2. Optical and scanning electron microscopy (SEM) micrographs of the cantilevers.

Cantilever vibrational characteristics are measured with the *optical lever* technique (Fig. 2). The position of a focused laser beam reflected off the top side of the cantilever onto a position sensitive detector (PSD) is monitored. The current output of the PSD was amplified and converted into a voltage output, sent to a lock-in amplifier (EG&G 7260) for signal extraction and filtering, and stored to a personal computer (PC), together with the stimulus signal for the function generator. The procedure is controlled in a LABVIEW® environment.

V. EXPERIMENTAL RESULTS AND DISCUSSION

In Fig. 3 we show an example of experimental resonance curves obtained for different pressure values. We can clearly see, moving from atmospheric pressure to high vacuum, both the shift of the resonance frequency towards higher values and then, when ω_r has reached its undamped value ω_0, the variation (decreasing) of the bandwidth.

From the resonance curve we can evaluate the quality factor as

$$Q = \frac{\omega_{\mathrm{peak}}}{\Delta\omega_{\mathrm{peak}}}, \tag{12}$$

where ω_{peak} is the maximum and $\Delta\omega_{\mathrm{peak}}$ is the width of the curve, evaluated for a 3 dB attenuation from the peak value.

As we said, we can divide the pressure range in three different regions, comparing the mean free path of the molecules and the dimension of the beam (the width of the cantilever, in our case). Due to the dimensions of our cantilevers (100 wide in the worst case), we can consider to work in the

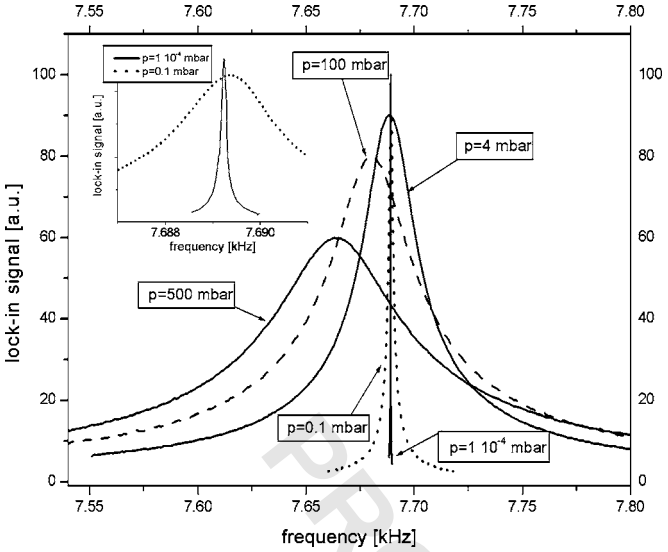

FIG. 3. Experimental resonance spectra for different pressure values. The dimensions of the cantilever beam are $800\times100\times5$ μm^3.

molecular flow region for pressures ranging from high vacuum limit (e.g., 10^{-3} Pa) to 100 Pa (the fine vacuum zone), and to be in the viscous region from 100 Pa to atmospheric pressure (the rough vacuum zone). Under 10^{-3} Pa down to 10^{-5} Pa (the maximum vacuum value we can obtain with our pumping system) there is the intrinsic region (high vacuum zone). Obviously, this is not an accurate division, and around 100 Pa a transition regime is located, in which it is difficult to understand what is the most accurate model to use.

In Fig. 4 we show the quality factor for a single-crystal rectangular-shape silicon cantilever (geometrical dimensions: 800 μm long, 100 μm wide, and 5 μm thick) as a function of the pressure, for the total range from high vacuum limit to

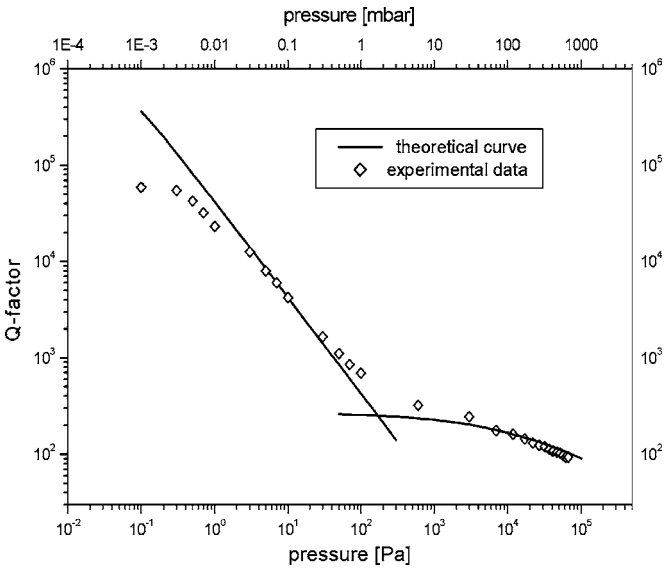

FIG. 4. Experimental evaluation for the quality factor (open diamonds) as a function of the pressure and comparison with the theoretical curve (solid line). The dimensions of the cantilever beam are $800\times100\times5$ μm^3.

atmospheric pressure (molecular and viscous regions). A comparison with the theoretical curves is presented. To obtain the theoretical curve in the molecular region ($Q_p \propto 1/p$) we used (4), (8), and (9), while in the viscous region (where, approximately, $Q_p \propto 1/\sqrt{p}$) we used (7)–(9). It is simple to evaluate that the clamping effects and TED contributions to Q are negligible. In our analysis we did not consider (10) and (11), because they contain parameters that are difficult to estimate.

We found a good agreement between calculated estimations and experimental values: a considerable difference is relieved for pressures below 0.1 Pa, where the contribution of internal frictions becomes predominant and experimental data present a saturation that we are not able to evaluate theoretically. We want here to emphasize that, for a pressure of 10^{-5} Pa (intrinsic region, not shown in Fig. 4), we obtain a resonance peak curve with a bandwidth of about 0.1 Hz, which is very close to the frequency resolution limit of our piezoelectric actuator.

Some differences between theory and experiment are also present in the transition region, around 100 Pa. In particular, our data show a pressure sensitivity also in the first part of the viscous regime (between 100 and 1000 Pa) and they do not show with clear evidence the plateau predicted by Blom *et al.*[19] In fact, for a 100 μm wide oscillator it is not completely correct to consider a zone in which the quality factor is independent of pressure because, neglecting the pressure dependence of the second term in the denominator of (7), we introduce an error greater than 10% (using the words of Blom *et al.*, we cannot consider the geometrical dimension of the cantilever, e.g., the radius of the sphere that we use to approximate the system, much smaller than the dimension of the turbulent region around the beam). So, the pressure effect in the quality factor evaluations are not negligible and give a dynamics in all the viscous region; the pressure-dependent trend in the transition regime is also confirmed in various experimental works in literature.[1,2,18,22,28] To confirm the difficulties to obtain a precise evaluation in the transition region, the error bars for these experimental points are greater (we can define the error bars starting from the hysteresis measurements shown below) than on the other pressure zones (except for the high vacuum region). In this pressure range it is difficult to give a precise theoretical description because of the superposition of different physical phenomena, but we are confident that our experimental data are not in contrast with the theoretical evaluations.

In Fig. 5 we present the normalized variation of the angular resonance frequency as a function of the pressure in the viscous region, for the same rectangular cantilever used above. We underline again a very good correspondence (except for the ambient pressure data) with the theoretical curve, obtained using (6).

So, data from Figs. 4 and 5 show that some important pressure-related drag effects are detectable using oscillating microcantilevers. The combination of information obtained from Q-factor evaluations and resonance frequency measurements gives us the possibility to obtain a certain pressure

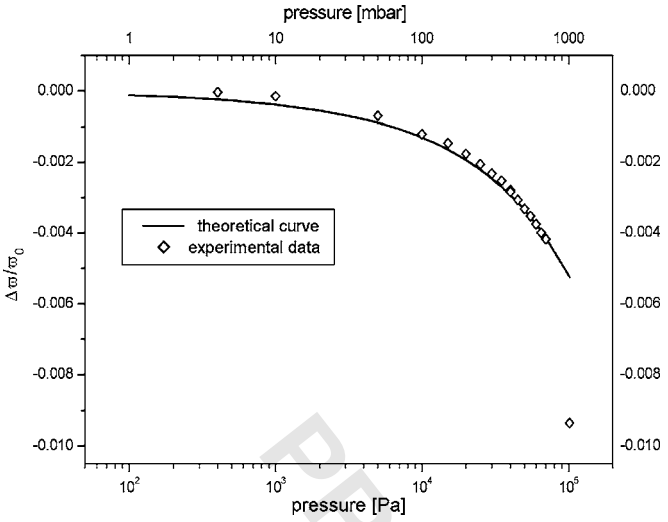

FIG. 5. Experimental evaluation for the normalized variation of the angular resonance frequency as a function of the pressure in the viscous region (open diamonds) and comparison with the theoretical curve (solid line). The dimensions of the cantilever beam are $800\times100\times5$ μm^3.

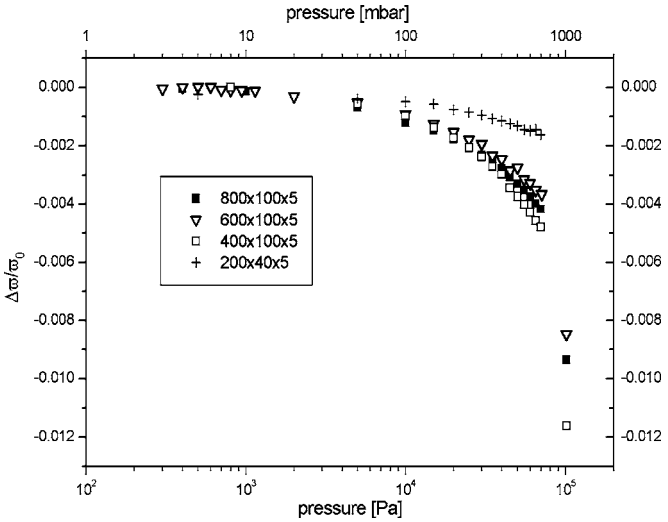

FIG. 7. Comparisons of pressure response for different cantilevers in viscous region. Geometrical dimensions are, as usual, (length) $\times$ (width) $\times$ (thickness) μm^3.

sensitivity over six decades (approximately from 0.1 to 10^5 Pa) using Q-related information from 0.1 to 10^3 Pa and $\Delta\omega$-related information for the last two decades.

Following this idea we evaluated the pressure response of rectangular-shape silicon cantilevers with different geometrical dimensions. In Fig. 6 we present the quality factor evaluations for three different cantilevers in fine vacuum conditions. To better show the difference between the samples we did a linear fit on two zones, to evaluate where the saturation ends and the pressure-dependent effect starts to be detectable. We can see, focusing our attention to the most critical zone (near 0.1 Pa), that the best results are obtained with the longest beam, which presents a slightly (but repeatable) wider response near this pressure value (the pressure sensitivity completely disappears around 0.2 Pa), while the others give a quite flat curve up to 1 Pa or more.

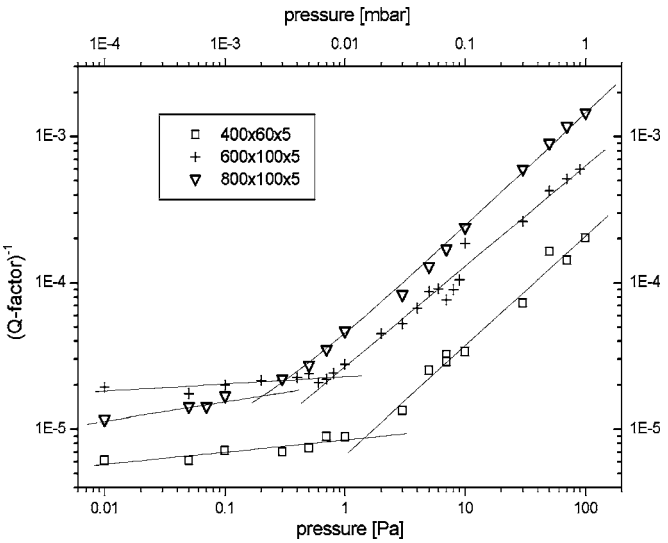

FIG. 6. Comparisons of pressure response for different cantilevers in molecular region. Drawn lines are fit of experimental values. Geometrical dimensions are, as usual, (length) $\times$ (width) $\times$ (thickness) μm^3.

In Fig. 7 we show the results for a similar analysis, evaluating the $\Delta\omega$ variation for different cantilever beams. Although there are some differences, in this case we can consider that all the analyzed cantilevers show the same behavior.

At last we evaluated the hysteresis behavior, studying the vibration response at various pressures moving first from high vacuum up to atmospheric pressure and then in the opposite direction. In Fig. 8 we can see the results of these analysis, noting that hysteresis effects are relieved in Q measurements only for higher vacuum conditions (pressure values lower than 0.1 Pa), and no hysteresis effects are appreciable for $\Delta\omega$ evaluations in the viscous pressure zone.

So, using a vibrating cantilever as a pressure sensor, we can obtain reliable and repeatable measurements even after many pumping cycles in a wide pressure range. The difference between the two experimental curves can be considered as the error of the measurement. As we underlined above, experimental errors for the Q-factor evaluation are greater in the high vacuum region and in the transition regime.

VI. CONCLUSIONS AND FUTURE DEVELOPMENTS

We produced rectangular silicon microcantilevers through a two-mask bulk micromachining process. These microstructures have been excited to resonance to exploit their capacitance to measure absolute pressure. We demonstrated that a silicon resonating microcantilever has the potential to perform absolute pressure measurements over a six decade range, according to its resonance frequency or quality factor shifts. Theoretical evaluations have been carried out to foresee the behavior of the microcantilever in molecular and vis-

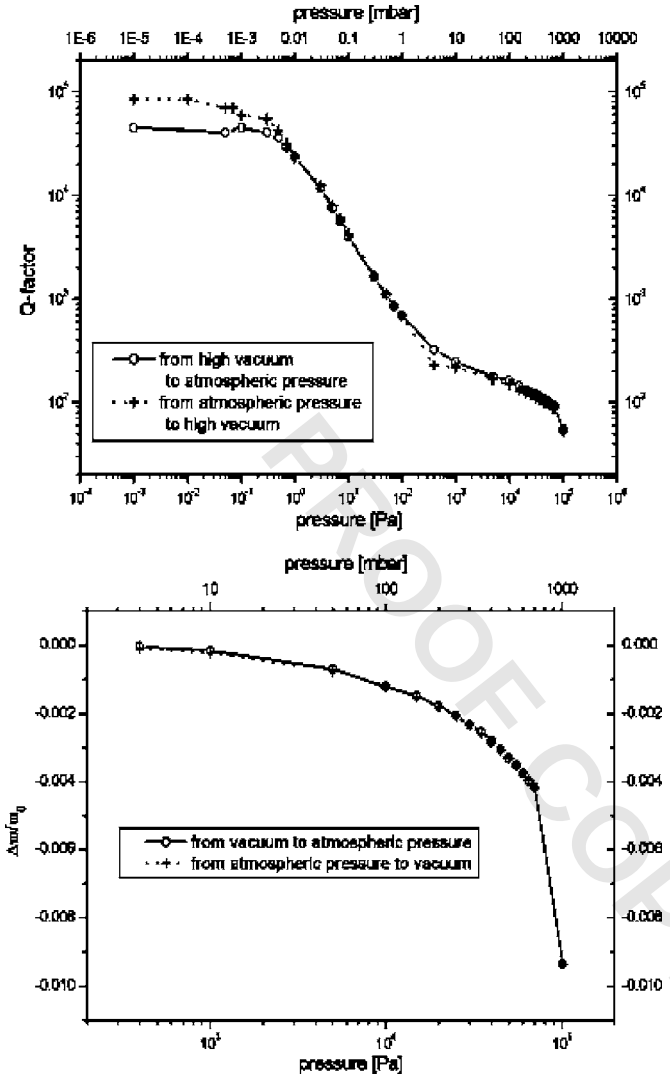

FIG. 8. Hysteresis curves for quality factor and normalized resonance frequency. The dimensions of the cantilever beam are $800 \times 100 \times 5\ \mu m^3$.

cous regimes. The obtained results are in good agreement with experimental data, thus providing a powerful instrument for the design.

Actually a SOI wafer technological solution is under investigation to upgrade the process. Work in progress is also focused on the development of an integrated solution including excitation and sensing (both capacitive and piezoresistive) for the fabrication of a complete absolute pressure sensor prototype. In this framework simulations with the finite element analysis (FEA) COVENTORWARE™ are deeply exploited to obtain useful elements for the design of the masks and this process.

ACKNOWLEDGMENTS

The research was supported by Varian SpA, through its R&D Laboratory located in Leinì (Turin-Italy). Moreover, special acknowledgements to Dr. John Helmer for his useful discussions and comments during the preparation of this work.

[1] J. Mertens, E. Finot, T. Thundat, A. Fabre, M. H. Nadal, V. Eyraud, and E. Bourillot, Ultramicroscopy **97**, 119 (2003).
[2] H. Kumazaki, S. Inaba, and K. Hane, Vacuum **47**, 475 (1996).
[3] J. Fricke and E. Obermeier, J. Micromech. Microeng. **3**, 190 (1992).
[4] B. H. Kim, M. Maute, F. E. Prins, D. P. Kern, M. Croitoru, S. Raible, U. Weimer, and W. Gopel, Microelectron. Eng. **53**, 229 (2000).
[5] J. Yang, T. Ono, and M. Esashi, Sens. Actuators, A **82**, 102 (2000).
[6] M. K. Baller *et al.*, Ultramicroscopy **82**, 1 (2000).
[7] A. Vidic, D. Then, and C. Ziegler, Ultramicroscopy **97**, 407 (2003).
[8] F. M. Battiston, J.-P. Ramseyer, H. P. Lang, M. K. Baller, C. Gerber, J. K. Gimzewski, E. Meyer, and H.-J. Guntherodt, Sens. Actuators B **77**, 122 (2001).
[9] J. Tamayo, M. Alvarez, and L. M. Lechuga, Sens. Actuators B **89**, 33 (2003).
[10] M. D. Antonik, N. P. D'Costa, and J. H. Hoh, IEEE Eng. Med. Biol. Mag. **66**, ■ (1997).
[11] P. Frederix, T. Akiyama, U. Staufer, C. Gerber, D. Fotiadis, D. J. Muller, and A. Engel, Curr. Opin. Chem. Biol. **7**, 641 (2003).
[12] H. X. You, J. M. Lau, S. Zhang, and L. Yu, Ultramicroscopy **82**, 297 (2000).
[13] S. Petitgrand, B. Courbet, and A. Bosseboeuf, J. Micromech. Microeng. **13**, 113 (2003).
[14] Y. Yee, M. Park, and K. Chun, J. Microelectromech. Syst. **7**, 339 (1998).
[15] D. Herman, M. Gaitan, and D. DeVoe, Proceedings of SEM Conference, Portland, OR, 2001 (unpublished).
[16] W. Choi and J. G. Smits, J. Microelectromech. Syst. **2**, 82 (1993).
[17] C. J. Kim, J. Y. Kim, and B. Sridharan, Sens. Actuators, A **64**, 17 (1998).
[18] K. Y. Yasumura, T. D. Stowe, E. M. Chow, T. Pfafman, T. W. Kenny, B. C. Stipe, and D. Rugar, J. Microelectromech. Syst. **9**, 117 (2000).
[19] F. R. Blom, S. Bouwstra, M. Elwenspoek, and J. H. J. Fiuitman, J. Vac. Sci. Technol. B **10**, 19 (1992).
[20] L. D. Landau and E. M. Lifshitz, *Course of Theoretical Physics*, 2nd ed. (Butterworth Washington, DC/Heinemann, London, 1987), Vol. 6, pp. 44–51, pp. 83–92.
[21] R. G. Christian, Vacuum **16**, 175 (1966).
[22] M. Bao, H. Yang, H. Yin, and Y. Sun, J. Micromech. Microeng. **12**, 341 (2002).
[23] K. Kokubun, M. Hirata, M. Ono, H. Murakami, and Y. Toda, J. Vac. Sci. Technol. A **5**, 2450 (1987).
[24] H. Hosaka, K. Itao, and S. Kuroda, Sens. Actuators, A **49**, 87 (1995).
[25] Z. Hao, A. Erbil, and F. Ayazi, Sens. Actuators, A **109**, 156 (2003).
[26] R. Lifshitz and M. L. Roukes, Phys. Rev. B **61**, 5600 (2000).
[27] J. Yang, T. Ono, and M. Esashi, J. Microelectromech. Syst. **11**, 775 (2002).
[28] S. Hutcherson and W. Ye, J. Micromech. Microeng. **14**, 1726 (2004).